

# Geophysical Research Letters®



## RESEARCH LETTER

10.1029/2023GL104146

## Effects of Composite Rheology on Plate-Like Behavior in Global-Scale Mantle Convection

Maëlis Arnould<sup>1,2</sup> , Tobias Rolf<sup>2,3</sup> , and Antonio Manjón-Cabeza Córdoba<sup>2,4,5</sup> 

<sup>1</sup>University of Lyon, UCBL, ENSL, UJM, CNRS UMR 5276, Laboratoire de Géologie de Lyon - Terre, Planètes, Environnement, Lyon, France, <sup>2</sup>Centre for Earth Evolution and Dynamics, Department of Geosciences, University of Oslo, Blindern, Oslo, Norway, <sup>3</sup>Institute of Geophysics, University of Münster, Münster, Germany, <sup>4</sup>Andalusian Earth Sciences Institute, University of Granada, Granada, Spain, <sup>5</sup>Department of Earth Sciences, University College London, London, UK

### Key Points:

- Uppermost mantle viscosity variations induced by composite rheology control surface tectonics
- Composite rheology can impede or enhance plate mobility depending on lithospheric strength
- Composite rheology does not facilitate the onset of subduction for large yield stress

### Supporting Information:

Supporting Information may be found in the online version of this article.

### Correspondence to:

M. Arnould,  
[maelis.arnould@univ-lyon1.fr](mailto:maelis.arnould@univ-lyon1.fr)

### Citation:

Arnould, M., Rolf, T., & Manjón-Cabeza Córdoba, A. (2023). Effects of composite rheology on plate-like behavior in global-scale mantle convection. *Geophysical Research Letters*, 50, e2023GL104146. <https://doi.org/10.1029/2023GL104146>

Received 19 APR 2023

Accepted 23 JUN 2023

**Abstract** Earth's upper mantle rheology controls lithosphere-asthenosphere coupling and thus surface tectonics. Rock deformation experiments and seismic anisotropy measurements indicate that composite rheology (co-existing diffusion and dislocation creep) occurs in the Earth's uppermost mantle, potentially affecting convection and surface tectonics. Here, we investigate how the spatio-temporal distribution of dislocation creep in an otherwise diffusion-creep-controlled mantle impacts the planform of convection and the planetary tectonic regime as a function of the lithospheric yield strength in numerical models of mantle convection self-generating plate-like tectonics. The low upper-mantle viscosities caused by zones of substantial dislocation creep produce contrasting effects on surface dynamics. For strong lithosphere (yield strength > 35 MPa), the large lithosphere-asthenosphere viscosity contrasts promote stagnant-lid convection. In contrast, the increase of upper mantle convective vigor enhances plate mobility for lithospheric strength <35 MPa. For the here-used model assumptions, composite rheology does not facilitate the onset of plate-like behavior at large lithospheric strength.

**Plain Language Summary** Understanding uppermost mantle flow and deformation is important to study Earth's surface evolution, since plate tectonics and mantle convection are intertwined processes. Observations and experiments provide important—yet uncertain—constraints suggesting that uppermost mantle viscosity should be at least partially controlled by dislocation creep (i.e., rheology should vary non-linearly with stress). However, most studies have not included dislocation creep. Here, we incorporate different amounts of this deformation mechanism in global-scale numerical models of mantle convection featuring Earth-like tectonic plates. We demonstrate that fast-evolving low-viscosity areas containing dislocation creep arise around slabs and plumes. Moreover, large amounts of dislocation creep alter surface tectonics in several ways: for a weak lithosphere, subductions become shorter-lived and plate velocities increase. For a strong lithosphere, in contrast, plate tectonics is inhibited. This study therefore demonstrates the key role of composite rheology in understanding mantle-lithosphere interactions.

## 1. Introduction

The lithospheric behavior of terrestrial bodies notably depends on their mantle properties and dynamics (e.g., Alisic et al., 2012; Coltice et al., 2017; Garel et al., 2020). In particular, mantle rheology determines the coupling between the convecting mantle and the lithosphere, therefore affecting surface heat transfer, plate velocities and continental motions (e.g., Rolf et al., 2018; Stein et al., 2004). Rock-deformation laboratory experiments conducted at upper-mantle conditions (Figures 1a and 1b, e.g., Hirth & Kohlstedt, 2003; Karato & Wu, 1993) show that mantle rheology is composite, meaning that deformation is driven by a coexistence of different creep mechanisms such as diffusion creep (linear or Newtonian stress/strain-rate dependence) and dislocation creep (non-linear power-law or non-Newtonian stress/strain-rate relationship). These experimental results are corroborated by the observed spatial heterogeneity in the strength of uppermost-mantle seismic anisotropy (e.g., Beghein et al., 2014; Debayle & Ricard, 2013), which could be at least partially explained by different amounts of olivine lattice preferred orientations (LPO), possibly caused by the heterogeneous development of dislocation creep in the uppermost mantle (e.g., Becker et al., 2006; Hedjazian et al., 2017; Nicolas & Christensen, 1987).

While mantle composite rheology is typically considered in regional-scale geodynamics models (e.g., Billen & Hirth, 2005; Garel et al., 2020; Neuharth & Mittelstaedt, 2023), it is often neglected in global-scale models (e.g.,

© 2023. The Authors.

This is an open access article under the terms of the [Creative Commons Attribution-NonCommercial-NoDerivs License](https://creativecommons.org/licenses/by-nc-nd/4.0/), which permits use and distribution in any medium, provided the original work is properly cited, the use is non-commercial and no modifications or adaptations are made.

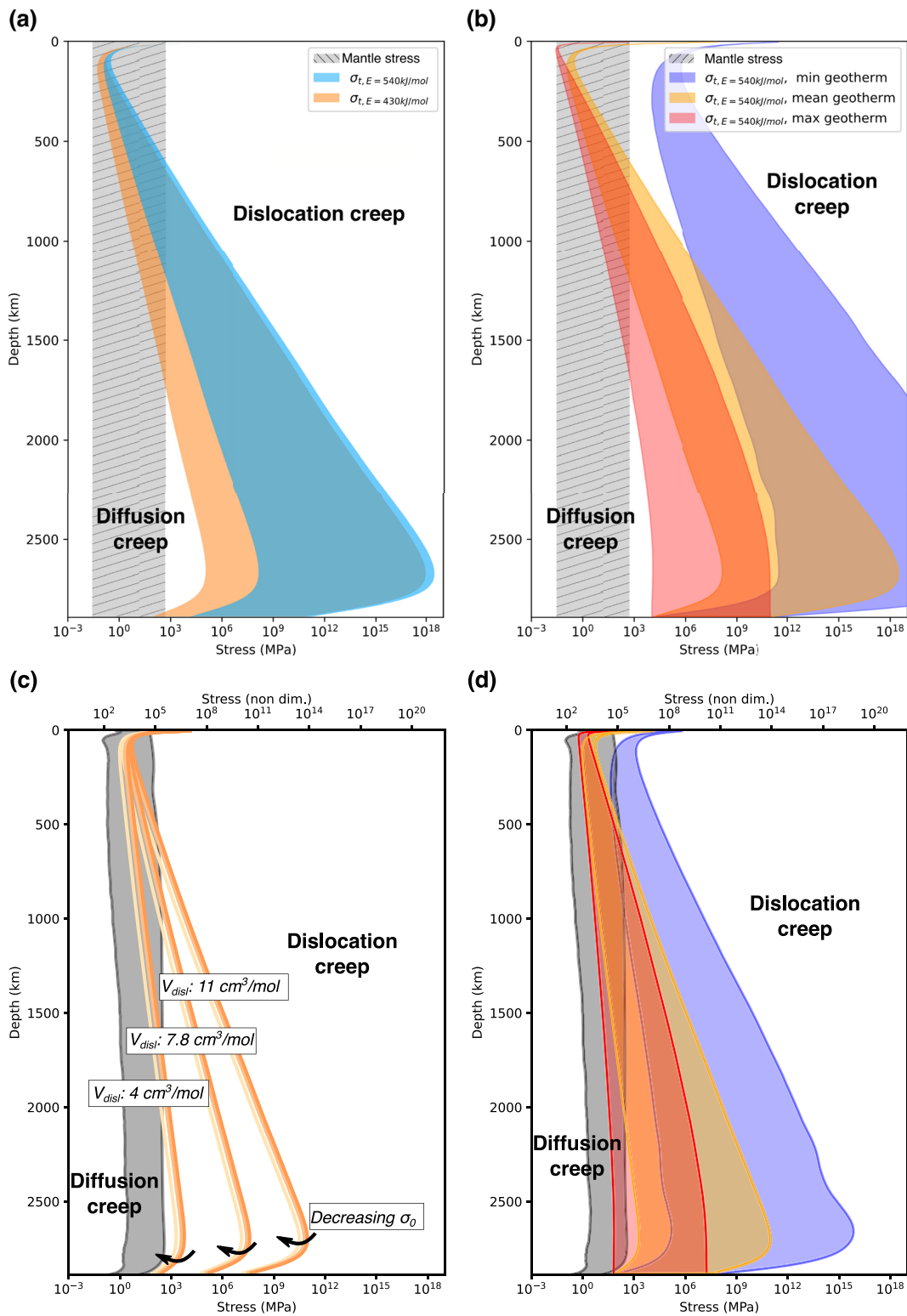


**Figure 1.** *Top:* Range of olivine transition stress measured by Karato and Wu (1993), assuming a grain-size of 1 mm. (a) Sensitivity to  $E_{disl}$  (blue: 430 and orange: 540  $\text{kJ mol}^{-1}$ ) and  $V_{disl}$  ( $10\text{--}25 \text{ cm}^3 \text{ mol}^{-1}$ ), using an average geotherm from a reference model in pure diffusion creep (Figure S1e in Supporting Information S1). (b) Sensitivity to temperature using  $E_{disl} = 430 \text{ kJ mol}^{-1}$  and  $10 < V_{disl} < 25 \text{ cm}^3 \text{ mol}^{-1}$  (blue = cold, yellow = average, and red = hot geotherm (Figure S1e in Supporting Information S1)). *Bottom:* Same as above, but for our modeling setup. (c) Sensitivity of the model transition stress to  $V_{disl}$  ( $4\text{--}11 \text{ cm}^3 \text{ mol}^{-1}$ ) and  $\sigma_0$  ( $1.2\text{--}3.5 \text{ MPa}$ ), using an average geotherm (Figure S1e in Supporting Information S1). (d) Sensitivity to temperature. In all panels, gray-striped areas show the stress range expected in Earth's mantle (top) and predicted in our reference model (bottom, Figure S1b in Supporting Information S1).

Coltice et al., 2017; Li & Zhong, 2019; Stein et al., 2004), or simply mimicked by reduced activation energy in pure diffusion creep rheology (Christensen, 1983, 1984). However, this latter approximation causes differences in the planform of stagnant-lid convection compared to using full composite rheology (e.g., Schulz et al., 2020). Moreover, prescribing pure diffusion creep makes it difficult to fully capture Earth's lithosphere and mantle behavior, such as observed plume swells' shapes (Asaadi et al., 2011), trench retreat rates (Holt & Becker, 2016), seismic anisotropy patterns around slabs (Jadamec & Billen, 2010), surface dynamic topography amplitudes (e.g., Bodur & Rey, 2019), and subduction geometry during its initiation (e.g., Billen & Hirth, 2005). Numerical studies prescribing pure dislocation creep in the upper-mantle have shown its importance for all these processes. However, in a composite formulation, the spatio-temporal distribution of the different creep mechanisms is not determined a priori, but arises self-consistently. Accounting for it therefore allows us to evaluate where substantial dislocation creep may occur in the mantle and to further study its effects on geodynamic processes. Some global models of mantle convection with plate-like behavior recently included composite rheology (e.g., Dannberg et al., 2017; Rozel, 2012), but these computationally demanding models used a single set of rheological activation parameters based on experimental values, while estimates vary over a large range (e.g., Jain et al., 2018, 2019; Korenaga & Karato, 2008; Ranalli, 2001). Moreover, these numerical studies focussed on the effect of grain-size evolution on the planform of convection and on the lithospheric behavior. Therefore, a systematic exploration of the effects of composite rheology in the upper mantle is still needed.

Here, we explore how the temperature-, depth-, and stress-dependent diffusion/dislocation creep partitioning impacts the planform of convection and the tectonic regime in 2D-cartesian whole-mantle convection models with composite rheology and static grain-size self-generating plate tectonics. Our goal is not to use Earth-like rheological parameters, but rather investigate the geodynamic effects of different parametrizations of composite rheology and capture qualitative convective and tectonic trends relevant for the Earth (Figure 1). We find that composite rheology influences both mantle convective planform and surface tectonics due to its spatio-temporal dynamic effect on uppermost mantle viscosity, either enhancing or altering plate mobility and plateness depending on lithospheric strength. These results demonstrate that uncertainties in experimentally-determined rheological parameters lead to substantial geodynamical effects, and call for further consideration of composite rheology in studies of mantle-lithosphere interactions.

## 2. Methods

### 2.1. On the Use of Composite Rheology

Mantle viscosity varies with temperature ( $T$ ), pressure ( $P$ ), grain-size ( $d$ ), and stress ( $\sigma$ ) (e.g., Hirth & Kohlstedt, 2003; Karato & Wu, 1993):

$$\eta_{mech} = A_{mech} d^m \sigma^{1-n} \exp\left(\frac{E_{mech} + PV_{mech}}{RT}\right). \quad (1)$$

$R$  is the gas constant,  $m$  is the grain-size exponent, and  $n$  is the stress exponent.  $E_{mech}$ ,  $V_{mech}$ , and  $A_{mech}$  are respectively the activation energy, the activation volume and a pre-exponential factor (accounting for all other effects on mantle rheology, such as water and melt content) for the rheological mechanism ( $mech$ ) considered (diffusion or dislocation creep).

Diffusion creep dominates below and dislocation creep dominates above the transition stress ( $\sigma_t$ ) at which the strain-rates due to the two different mechanisms are equal ( $\dot{\epsilon}_{diff} = \dot{\epsilon}_{dist}$ , e.g., Christensen, 1984; Hall & Parmentier, 2003):

$$\sigma_t = \left(\frac{A_{diff}}{A_{dist}}\right)^{\frac{1}{n-1}} d^{-\frac{m}{n-1}} \exp\left(\frac{(E_{dist} - E_{diff}) + P(V_{dist} - V_{diff})}{RT}\right)^{\frac{1}{n-1}}. \quad (2)$$

$E_{diff}$ ,  $E_{dist}$ ,  $V_{diff}$ , and  $V_{dist}$  can be determined for olivine from rock experiments (e.g., Karato & Wu, 1993) and vary respectively between 240–450 and 430–560 kJ/mol, 0–20 and 0–33 cm<sup>3</sup>/mol (Hirth & Kohlstedt, 2003; Karato & Wu, 1993; Ranalli, 2001), depending on water content. Despite those uncertainties,  $E_{diff} < E_{dist}$  and  $V_{diff} < V_{dist}$  (Figures 1a and 1b, e.g., Karato & Wu, 1993). Those experiments predict that dislocation creep should dominate in hot regions of the uppermost-mantle and areas submitted to high stresses (Figures 1a and 1b).

## 2.2. Numerical Model Setup

We solve the non-dimensional equations of mass, momentum and energy conservation under the Boussinesq approximation using StagYY (e.g., Tackley, 2000a) on a 2D-cartesian  $512 \times 128$  or  $768 \times 192$  grid (aspect ratio 4:1). Grid cells are refined near the thermal boundary layers. Top and bottom boundaries are free-slip, lateral boundaries are periodic. We use a reference Rayleigh number of  $10^7$ . The mantle is heated both from below and from within (constant internal heating rate  $H = 8.6 \times 10^{-12}$  W kg $^{-1}$ , Table S1 in Supporting Information S1).

We use a pseudoplastic rheology to model plate-like behavior (e.g., Tackley, 2000a; Trompert & Hansen, 1998), and vary the surface yield stress  $\sigma_{Y_0}$ , which represents lithospheric strength, between 12 and 234 MPa. The yield stress varies with depth at a rate of  $\sim 0.3$  MPa km $^{-1}$ . The surface yield stress is bounded by the typical stress drop during earthquakes (10 MPa, Allmann & Shearer, 2009) and the yield stress of pristine lithospheric rocks measured in experiments (Brace & Kohlstedt, 1980). Over the modeled range of yield stresses, diverse tectonic behaviors are expected for pure diffusion creep: from mobile plates at low yield stress to stagnant-lid at high yield stress (e.g., Arnould et al., 2018).

In StagYY, the transition stress  $\sigma_t^*$  between diffusion and dislocation creep is defined in analogy to Equation 2 as:

$$\sigma_t^* = \sigma_0 \left( \frac{B_{disl}}{B_{diff}} \right)^{\frac{1}{n-1}} \left( \frac{d}{d_0} \right)^{-\frac{m}{n-1}} \exp \left( \frac{(E_{disl} - E_{diff}) + P(V_{disl} - V_{diff})}{R(T + T_0 - T_{surf})} \right)^{\frac{1}{n-1}}. \quad (3)$$

$T_0 = 0.64$  is the non-dimensional reference temperature, equivalent to 1,600 K and  $T_{surf} = 0.12$  is the non-dimensional surface temperature, equivalent to 300 K.  $\sigma_0$  is a reference transition stress.  $B_{diff}$  and  $B_{disl}$  differ from  $A_{mech}$  in Equation 1 and ensure that mantle viscosity equals the non-dimensional reference viscosity  $\eta_0 = 1$  ( $9.8 \times 10^{21}$  Pa s) at reference conditions (temperature of 1,600 K and surface pressure). As we do not account for grain-size evolution,  $d = d_0$  unless explicitly mentioned otherwise (see discussion in Section 4). For dislocation creep,  $m = 0$  and  $n = 3.5$  while for diffusion creep,  $m = 2$  and  $n = 1$ .

## 2.3. Computed Cases

For each value of  $\sigma_{Y_0}$ , we fix  $E_{diff}$ ,  $V_{diff}$  and  $E_{disl}$ , but vary  $V_{disl}$  by a factor of  $\sim 3$ , since its experimental value is subjected to the largest uncertainties (e.g., Karato & Wu, 1993; Korenaga & Karato, 2008). We also vary  $\sigma_0$  between 1.2 and 3.5 MPa to ensure that dislocation creep is mostly restricted to the upper mantle. We choose lower activation parameters than experimentally determined for pristine olivine for reasons of numerical feasibility. Instead, we preserve ranges of variation for  $E_{disl} - E_{diff}$  and  $V_{disl} - V_{diff}$  similar to rock experiments (Karato and Wu (1993); Figure 1) since these differences matter the most in Equations 2 and 3. The spatio-temporal evolution of mantle convection self-consistently partitions the mantle into areas dominated by dislocation creep or diffusion creep, depending on the level of stress.

For each yield stress, we first ran models in pure diffusion creep over 3 Gyr, starting from a stratified thermal field with small perturbations to initiate convection. We then restarted from the final thermal field of these models while including composite rheology and ran those new models over 3 Gyr. Since we do not model evolutionary models, this procedure ensures that the models are in quasi-statistical steady-state (Figure S2 in Supporting Information S1) during the last 400 Myr of each simulation that we analyze. Detailed model parameters, with their non-dimensional and dimensional values are given in Table S1 in Supporting Information S1.

## 3. Results

### 3.1. Spatio-Temporal Distribution of Dislocation Creep

Decreasing both  $V_{disl}$  and/or  $\sigma_0$  results in a thicker and more continuous layer deforming in dislocation creep in the upper mantle (Figure 2). As a consequence, upper mantle viscosity decreases by at least one order of magnitude on average. Moreover, average horizontal and vertical velocities increase by a factor of 3 depending on the amount of dislocation creep (Figure 2a), irrespective of the surface yield stress (Figure S3 in Supporting Information S1), showing that composite rheology enhances convective vigor locally. Due to its location and low viscosity signature, the layer containing  $>10\%$  dislocation creep is here-after referred to as an ‘‘asthenosphere’’ in models with composite rheology, although it sometimes locally reaches lower-mantle depths (low  $V_{disl}$  and  $\sigma_0$ ).

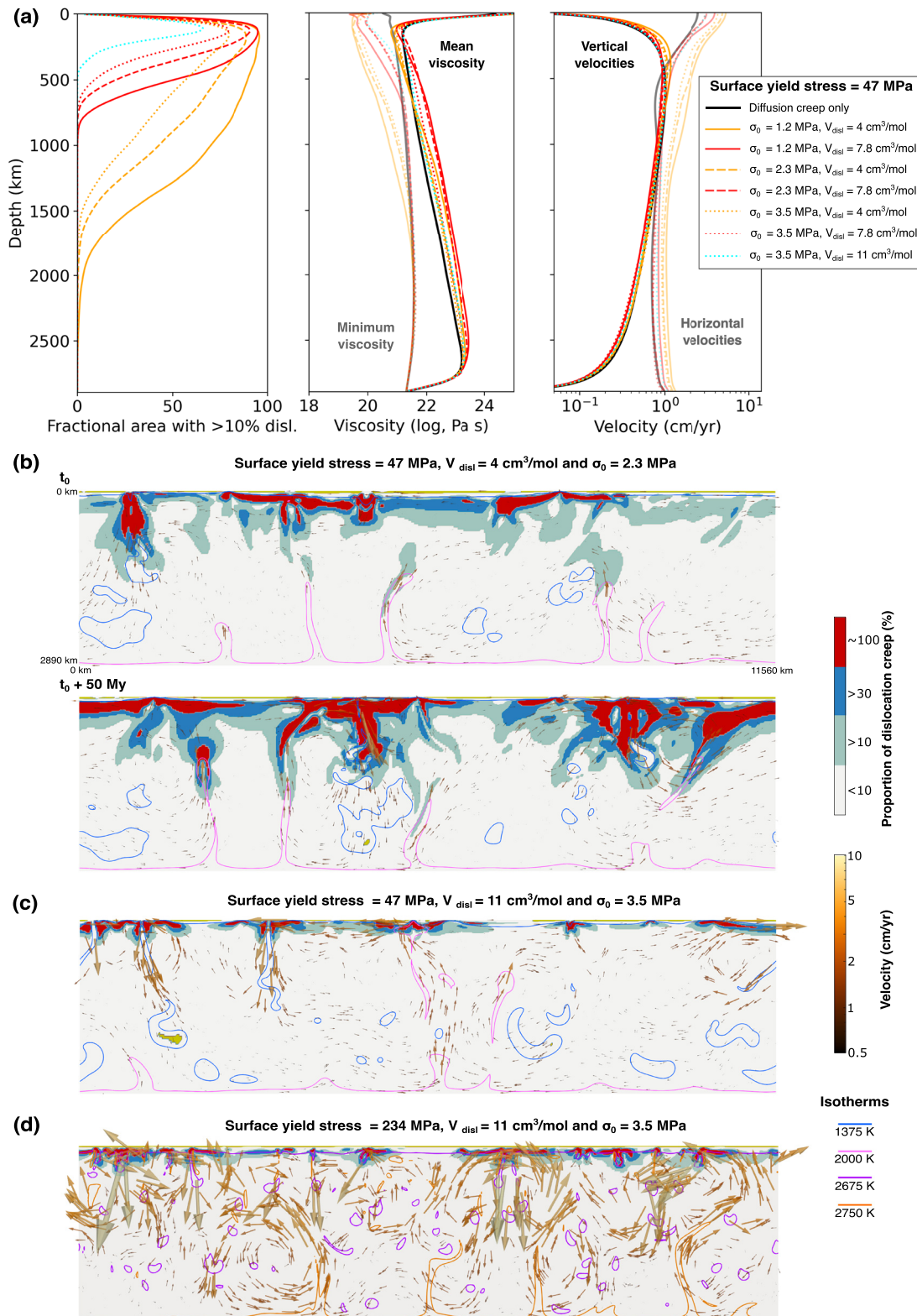


**Figure 2.** (a) Time-averaged profiles of (left) mantle fractional area with >10% dislocation creep, (middle) minimum and mean viscosity, and (right) vertical and horizontal velocity for models with a surface yield stress  $\sigma_0 = 47$  MPa. (b–d) Proportion of dislocation creep and mantle velocity field (arrows scaled and colored by magnitude) in three models. In (b), a 50 Myr-evolution is shown. In (b and c), blue lines show slabs and magenta lines contour plumes. In (d), purple lines contour dripping lithosphere and orange lines show hotter-than-average upwellings.

Areas strongly affected by dislocation creep show a high spatio-temporal variability within the asthenospheric layer (Figures 2b–2d and Movie S1), which produces large lateral viscosity variations in the upper mantle, as suggested by Alisic et al. (2012), Billen and Hirth (2007), Semple and Lenardic (2020), and others. In models featuring plate-like behavior, dislocation creep mainly occurs around slabs and plumes in the uppermost mantle. Indeed, ambient mantle shearing by sinking slabs is responsible for the highest convective stresses and thus for a higher proportion of dislocation creep around them. In contrast and depending on their thickness, slab interiors deform mostly through diffusion creep (Figures 2b and 2c) because of their much colder state (Figures 1b and 1d). The evolution of individual slabs is significantly affected by composite rheology, consistent with regional thermo-mechanical models (e.g., Garel et al., 2020): slabs tend to sink faster through an upper mantle with more abundant dislocation creep and thus a more pronounced low viscosity zone (Figure 2). Moreover, they tend to buckle and/or break-off more easily depending on their strength and the mantle viscosity structure (Figures 4a and 4d). In fact, both the amount of dislocation creep around slabs and the thickness of the asthenosphere are responsible for creating a viscosity contrast between the upper and the lower mantle, which hinders the sinking of slabs and affects their evolution (Figure 2a, e.g., Billen & Hirth, 2007).

Around plumes, hot mantle more likely deforms through dislocation creep (Figures 1b and 1d), although shearing is less important than around slabs. Plumes are thus also surrounded by lower viscosities than in pure diffusion creep cases, which favors fast rising (Figure 2 and Figure S4 in Supporting Information S1). Plume material further tends to feed fast lateral asthenospheric channelled-flow (as proposed by e.g., Phipps Morgan et al., 1995) in which dislocation creep occurs more likely due to high temperatures and stresses, favoring even lower viscosity in these areas than in diffusion creep models (Figures 2a and 2b). This occurs preferentially when new plume heads reach sub-lithospheric depths. Over a few million to a few tens of million years, the geometry and abundance of dislocation creep can therefore vary considerably (Figures 2b and 2c), controlled by the dynamics of convective thermal heterogeneities.

Models with a surface yield strength larger than 120 MPa experience stagnant-lid convection. In these models, the mantle is much warmer due to limited heat loss, thus favoring more vigorous and smaller-scale convection than in cases with plate-like behavior (Figure 2). Higher temperature and increased convective vigor promote dislocation creep, which emerges in areas of basal lithosphere dripping, or around hotter-than-average upwellings in the shallow mantle (Figure 2c). The large variability of these processes controls the spatio-temporal distribution of dislocation creep.

### 3.2. Effects on the Tectonic Regime

The effect of composite rheology on the surface tectonic regime is quantified through surface mobility  $M = \frac{v_{surf}}{v_{rms}}$  (with  $v_{surf}$  the average surface velocity and  $v_{rms}$  the volume root-mean-square velocity) and plateness  $P = 1 - \frac{def_{90}}{def_{90,iso}}$  (with  $def_{90}$  being the fractional surface area containing 90% of deformation, and  $def_{90,iso}$  being the value for an isoviscous model, Tackley, 2000a). These proxies are close to 1 for the mobile-lid regime and tend to 0 in the stagnant-lid regime, with episodic transitioning between these end-members. In addition, we track the number of active subduction zones, detected from surface downward velocity peaks, and the lithospheric thickness, defined from the inflection point of the time-averaged temperature profile (Figure 3 and Figure S5 in Supporting Information S1).

Regardless of the surface yield strength, lithosphere thickness decreases as the proportion of dislocation creep increases (Figure 3a and Figure S5 in Supporting Information S1), by up to 60% compared to diffusion creep models. In the asthenospheric areas strongly affected by dislocation creep, increased convective vigor tends to impede lithospheric growth due to more efficient convective erosion. Therefore, the thicker the layer with substantial dislocation creep, the thinner is the lithosphere for a given surface yield stress compared to pure diffusion-creep models. Beside the major control of surface lithospheric yield strength, composite rheology has two contrasting effects on the tectonic regime. These effects are summarized on Figures 4a–4c and described below.

#### 3.2.1. Models With a Weak Lithosphere (<35 MPa)

For yield stresses below ~35 MPa, models in pure diffusion creep are in the mobile-lid regime. Composite rheology enhances surface mobility (up to 1.6) and plateness. Active subduction zones tend to be shorter-lived

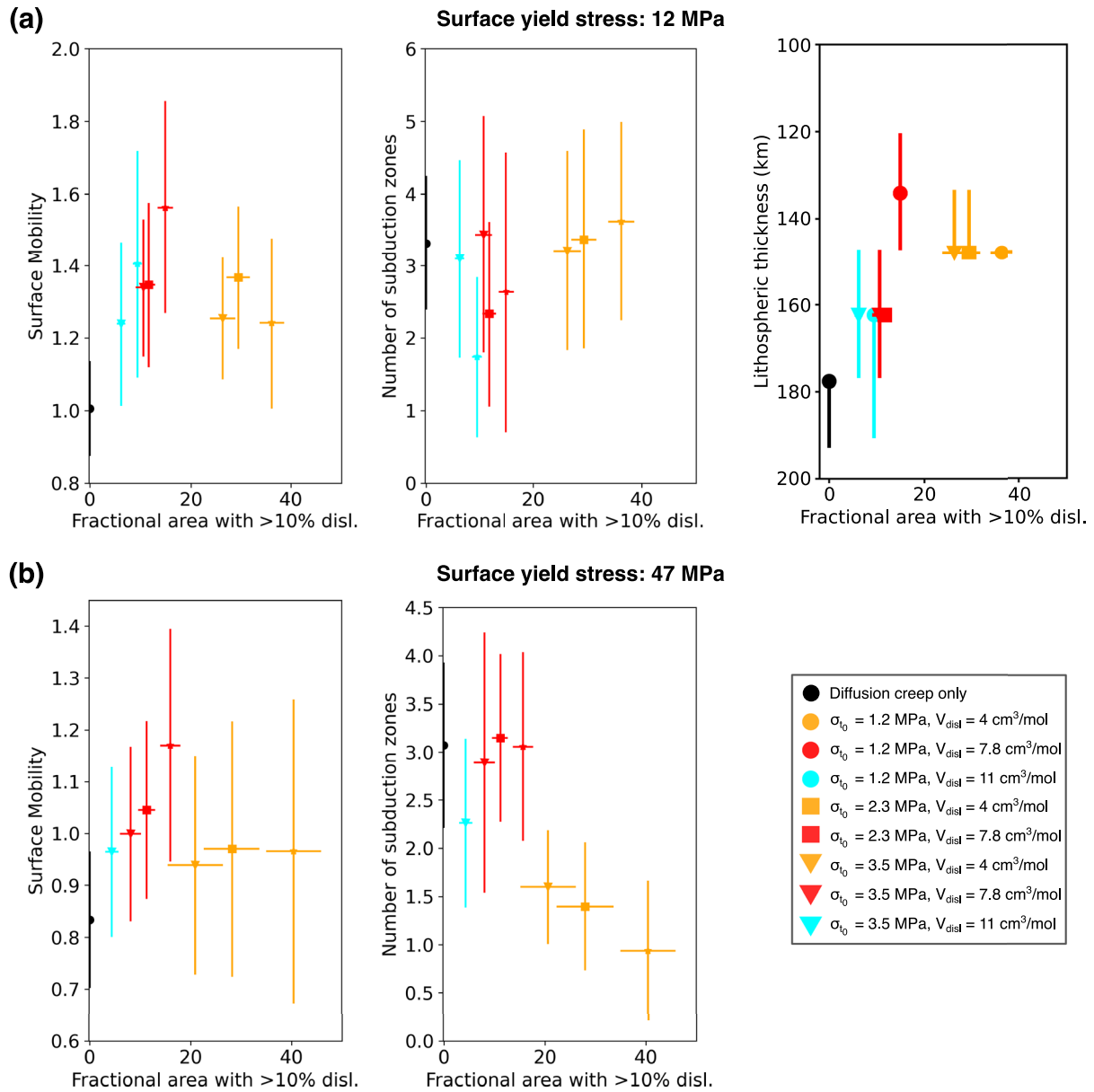


**Figure 3.** Effect of composite rheology on surface tectonic regime (temporal average and standard deviation of surface mobility, number of subduction zones, and lithosphere thickness as a function of the time-averaged mantle fractional area containing >10% dislocation creep) in models with (a)  $\sigma_{y0} = 12$  and (b) 47 MPa.

(Figure 4d). In these models, the viscosity reduction in the uppermost mantle induced by dislocation creep leads to decoupling of the lithosphere from the asthenosphere via lubrication, and to reduced stress acting on the lithosphere although local convective vigor increases (Tackley, 2000b). This decoupling contributes to the observed increase in mobility. Since dislocation creep also favors lithosphere thinning, the plastic strength at lithospheric base is reduced compared to models in pure diffusion creep. Therefore, an increasing amount of dislocation creep enhances thin slab break-offs. Accounting for composite rheology in models with a low lithospheric strength thus enhances mobile-lid convection.

### 3.2.2. Models With a Strong Lithosphere (>35 MPa)

Models in pure diffusion creep with surface yield stresses comprised between  $\sim 35$  and  $\sim 120$  MPa are also still in the mobile-lid regime. Including composite rheology using decreasing values of  $V_{disl}$  and/or  $\sigma_0$  results in up to 40% of the mantle being affected by dislocation creep (Figures 3b and 4a–4c).

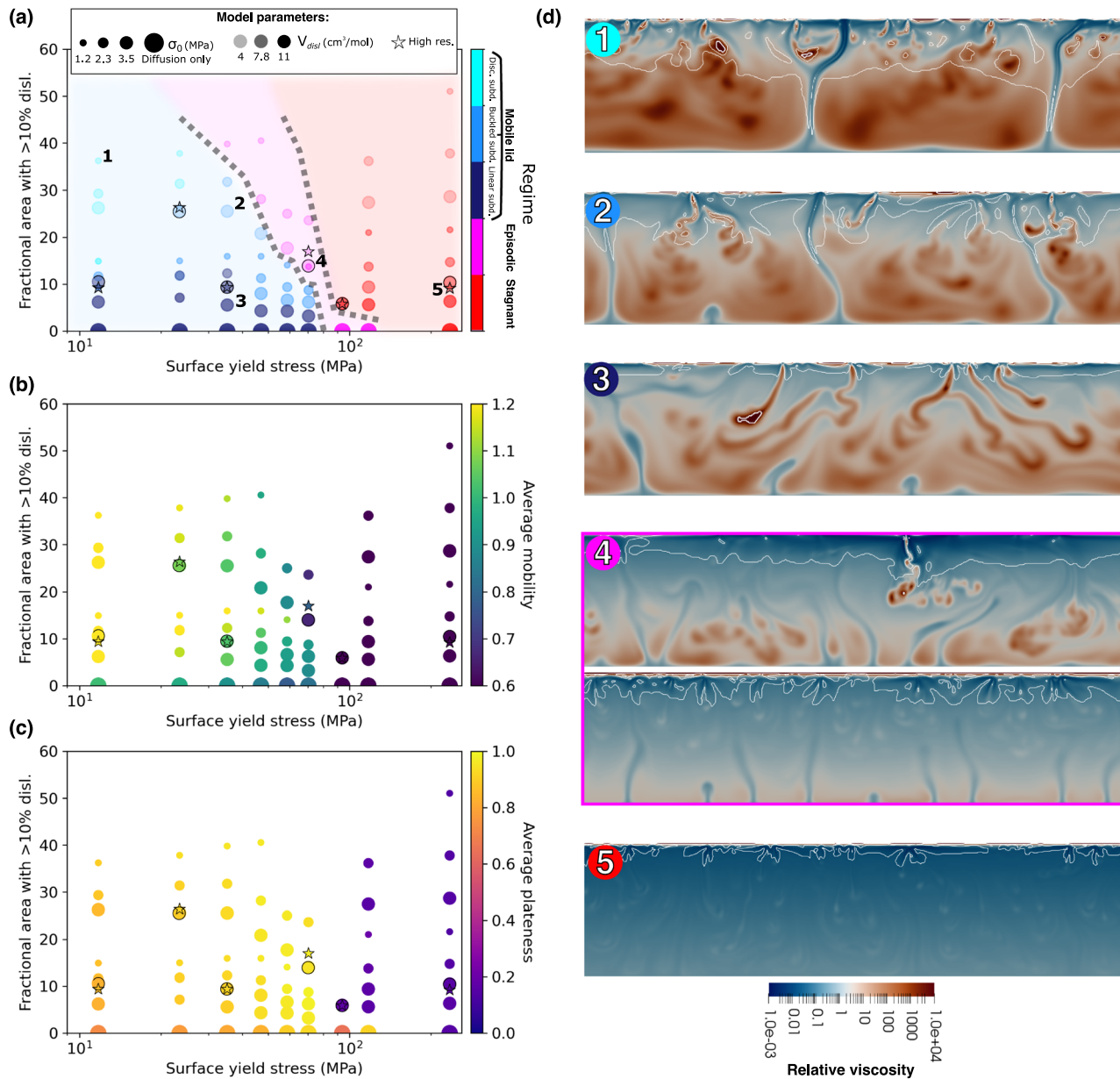


**Figure 4.** (a) Regime diagram of all models. Mobile-lid models have discontinuous and short-lived subductions (cyan), buckled slabs (blue), and or mostly linear slabs (deep-blue). Episodic models (magenta) have intermediate plateness and mobility. Stagnant-lid models (red) have low plateness and mobility. Qualitative boundaries are drawn between each regime. (b, c) Similar to (a) but with colors representing time-averaged surface mobility and plateness, respectively. Stars show the comparison between high-resolution models and lower-resolution models contoured in black. (d) Snapshots of viscosity of selected models referred as numbers in panel (a). White lines contour low-viscosity regions with >10% dislocation creep.

For small amounts of dislocation creep in the mantle (<20%), both plateness and surface mobility tend to increase by a factor of up to 1.4 and the number of slabs remains stable (Figure 3b). In these models, thin low-viscosity asthenospheric areas tend to lubricate the base of the lithosphere, enhancing plate mobility and plateness (e.g., Tackley, 2000b).

When the proportion of dislocation creep exceeds 20%, the number of active subductions, plateness and surface mobility decrease (Figures 3b and 4a–4c and Figure S5b in Supporting Information S1). Lithosphere–asthenosphere decoupling promotes episodic and stagnant-lid convection (Figure 4). This strengthening phenomenon due to large viscosity contrasts between the convecting mantle and the lithosphere has long been demonstrated using Newtonian rheology (e.g., Höink et al., 2012; Moresi & Solomatov, 1995; Solomatov, 1995, although the latter



study invoked a flow channelization effect as being responsible for stagnant-lid convection) and non-Newtonian rheology in the asthenosphere (Semple & Lenardic, 2020, although they did not employ temperature- and depth-dependent viscosity, in contrast to the present study).

We further tested higher surface yield stresses ( $>120$  MPa), which led to continuous stagnant-lid behavior irrespective of our choice of activation parameters. Like in models with a lower yield stress, decreasing  $V_{disl}$  and/or  $\sigma_0$  produces a thickening of the layer containing dislocation creep. Although the convective regime remains unchanged in these models, changing the amount of dislocation creep can strongly decrease the viscosity in the asthenosphere and decrease lithospheric thickness by up to 60%. These effects could have a large impact on the distribution of partial melting and the rates of magmatism on stagnant-lid planets (e.g., Schulz et al., 2020; Tosi & Padovan, 2021). However, these models also suggest that once a stagnant-lid is established with a pure diffusion creep rheology, adding composite rheology in the upper-mantle does not promote the generation of more plate-like behavior.

## 4. Discussion and Conclusion

### 4.1. Model Assumptions

Model setup simplifications potentially alter mantle flow and therefore the spatio-temporal diffusion/dislocation creep partitioning. Our models are limited to 2D-cartesian, have a reference Rayleigh number  $\sim 10$  times lower than Earth's, lower lithospheric strengths than inferred from laboratory experiments (e.g., Brace & Kohlstedt, 1980), and lower activation parameters for olivine than those predicted by rock experiments (e.g., Hirth & Kohlstedt, 2003). We do not consider multiple mantle and lithosphere compositions and phases (e.g., King, 2016). We also only tested one initial thermal state for our models with composite rheology although different initial conditions could lead to distinct regime boundaries for diffusion-creep-only and composite rheology, as notably shown in Semple and Lenardic (2021) and Weller and Lenardic (2018).

However, our mobile-lid models still produce mantle velocities on the order of the cm/yr (Figure 2a), oceanic lithosphere thickness of 100–200 km, and successfully generate dislocation creep where it is expected to occur from rock-deformation experiments although we use lower  $E_{mech}$  (Figure 1). We also note no significant difference when increasing the resolution (Figures 4a–4c, star symbols). Therefore, we anticipate that the general convective and tectonic trends (Figure 4) and physical mechanisms described in this study still apply using more Earth-like setups. In particular, we obtain a self-generated and self-evolving low-viscosity asthenosphere without invoking water and/or partial melting (King, 2016; Semple & Lenardic, 2020), the latter being often called on to justify the use of weakening laws to improve flatness in whole-mantle Newtonian models (e.g., Bello et al., 2015; Tackley, 2000a).

Importantly, we assumed a uniform static grain-size, although rock-deformation experiments indicate that diffusion creep should strongly depend on grain-size evolution (Equation 1). In some stagnant-lid models, we increased the static grain-size, which produced an increase in mantle average viscosity, stress, and proportion of dislocation creep in the uppermost mantle (Figure S6 in Supporting Information S1), associated with lithospheric thickening, as already described in Schulz et al. (2020). This test, applied to models without dynamic grain-growth and reduction, reveals the competing effects of large grain-size (which tends to increase mantle viscosity) and large amounts of dislocation creep (which tend to decrease it) on lithosphere thickness, at least up to a doubling of static grain-size with our setup (Figure S6 in Supporting Information S1). Further exploring the role of grain-size evolution in mobile-lid scenarios is therefore needed to further understand the role of composite rheology on mantle and lithosphere dynamics.

### 4.2. Earth's Observations and Composite Rheology in the Uppermost Mantle

On Earth, seismic anisotropy, through the generation of dislocation creep-induced LPO (e.g., Nicolas & Christensen, 1987), can provide complementary insight on the lateral variations of mantle rheological properties (e.g., Becker et al., 2008). Although 3D modeling is required to quantitatively compare the diffusion/dislocation creep partitioning in our models with observed seismic anisotropy, our results already potentially explain its observed orientation and strength variations (e.g., Debayle et al., 2005), as well as high strength around slabs (e.g., Jadamec & Billen, 2012) and in the thermal trail of plumes (e.g., Barruol et al., 2019). The correlation

between strong anisotropy and fast plate velocities described in Debayle and Ricard (2013) could also partly result from the fact that these plates are attached to fast sinking slabs, thus favoring more dislocation creep due to lithospheric basal shear. One future direction would therefore be to estimate seismic anisotropy in more Earth-like models with composite rheology and compare it to Earth's observations (e.g., Kendall et al., 2022). Together with the consideration that some rheological parameters are inter-dependent (e.g., Jain et al., 2019), this should provide complementary constraints on the range of rheological parameters applicable to Earth. Another independent constraint could come from the study of how composite rheology affects the spatio-temporal distribution of surface dynamic topography, both on the long-term (e.g., Bodur & Rey, 2019) and on shorter glacial-isostatic-adjustment timescales (Kang et al., 2022).

In this study, we show that our choice of composite rheological parameters impacts uppermost mantle spatio-temporal viscosity variations and dynamics, therefore affecting convection and surface tectonics in a non-linear way: at low lithospheric strength, increasing the proportion of mantle deforming through dislocation creep promotes plate mobility as well as numerous, weaker and short-lived slabs. In contrast, increasing the proportion of mantle containing dislocation creep in models with large lithospheric strength, results in episodic to stagnant-lid convection. This shows the potential geodynamical influence of experimental uncertainties of the rheological parameters and calls for both further experimental refinement of mantle rheological parameters such as  $V_{disl}$  and further exploration of the effects of composite rheology on mantle convective planform and surface tectonics in more sophisticated planetary-scale models.

### Data Availability Statement

The convection code StagYY (Tackley, 2008) is property of ETH Zurich and Paul J. Tackley. Data files used in this study can be downloaded from Arnould (2022).

### Acknowledgments

This research benefited from Norwegian Research Council funding to the Centre for Earth Evolution and Dynamics (223272) and to TR (PLATONICS, 276032). MA benefited from CNRS-INSU-PNP and UCBL-BQR fundings. Computations were performed on Stallo and Saga Uninett Sigma2 facilities (nn9010k, ns9010k). Cramer et al. (2020) authored Figure 4d colormap.

### References

- Alisic, L., Gurnis, M., Stadler, G., Burstedde, C., & Ghattas, O. (2012). Multi-scale dynamics and rheology of mantle flow with plates. *Journal of Geophysical Research*, *117*(B10), 148–227. <https://doi.org/10.1029/2012JB009234>
- Allmann, B. P., & Shearer, P. M. (2009). Global variations of stress drop for moderate to large earthquakes. *Journal of Geophysical Research*, *114*(B1), B01310. <https://doi.org/10.1029/2008JB005821>
- Arnould, M. (2022). Effects of composite rheology on plate-like behaviour in global-scale mantle convection [Dataset]. OSF. <https://doi.org/10.17605/OSF.IO/P3MVN>
- Arnould, M., Coltice, N., Flament, N., Seigneur, V., & Muller, R. D. (2018). On the scales of dynamic topography in whole-mantle convection models. *Geochemistry, Geophysics, Geosystems*, *19*(9), 3140–3163. <https://doi.org/10.1029/2018GC007516>
- Asaadi, N., Ribe, N. M., & Sobouti, F. (2011). Inferring nonlinear mantle rheology from the shape of the Hawaiian swell. *Nature*, *473*(7348), 501–504. <https://doi.org/10.1038/nature09993>
- Barruol, G., Sigloch, K., Scholz, J.-R., Mazzullo, A., Stutzmann, E., Montagner, J.-P., et al. (2019). Large-scale flow of Indian Ocean asthenosphere driven by Réunion plume. *Nature Geoscience*, *12*(12), 1043–1049. <https://doi.org/10.1038/s41561-019-0479-3>
- Becker, T. W., Chevrot, S., Schulte-Pelkum, V., & Blackman, D. K. (2006). Statistical properties of seismic anisotropy predicted by upper mantle geodynamic models. *Journal of Geophysical Research*, *111*(B8), B08309. <https://doi.org/10.1029/2005JB004095>
- Becker, T. W., Kustowski, B., & Ekström, G. (2008). Radial seismic anisotropy as a constraint for upper mantle rheology. *Earth and Planetary Science Letters*, *267*(1–2), 213–227. <https://doi.org/10.1016/j.epsl.2007.11.038>
- Beghein, C., Yuan, K., Schmerr, N., & Xing, Z. (2014). Changes in seismic anisotropy shed light on the nature of the Gutenberg discontinuity. *Science*, *343*(6176), 1237–1240. <https://doi.org/10.1126/science.1246724>
- Bello, L., Coltice, N., Tackley, P. J., Müller, R. D., & Cannon, J. (2015). Assessing the role of slab rheology in coupled plate-mantle convection models. *Earth and Planetary Science Letters*, *430*, 191–201. <https://doi.org/10.1016/j.epsl.2015.08.010>
- Billen, M. I., & Hirth, G. (2005). Newtonian versus non-Newtonian upper mantle viscosity: Implications for subduction initiation. *Geophysical Research Letters*, *32*(19), L19304. <https://doi.org/10.1029/2005GL023457>
- Billen, M. I., & Hirth, G. (2007). Rheologic controls on slab dynamics. *Geochemistry, Geophysics, Geosystems*, *8*(8), Q08012. <https://doi.org/10.1029/2007GC001597>
- Bodur, Ö. F., & Rey, P. F. (2019). The impact of rheological uncertainty on dynamic topography predictions. *Solid Earth*, *10*(6), 2167–2178. <https://doi.org/10.5194/se-10-2167-2019>
- Brace, W. F., & Kohlstedt, D. L. (1980). Limits on lithospheric stress imposed by laboratory experiments. *Journal of Geophysical Research*, *85*(B11), 6248–6252. <https://doi.org/10.1029/JB085iB11p06248>
- Christensen, U. (1983). Convection in a variable-viscosity fluid: Newtonian versus power-law rheology. *Earth and Planetary Science Letters*, *64*(1), 153–162. [https://doi.org/10.1016/0012-821X\(83\)90060-2](https://doi.org/10.1016/0012-821X(83)90060-2)
- Christensen, U. (1984). Convection with pressure- and temperature-dependent non-Newtonian rheology. *Geophysical Journal International*, *77*(2), 343–384. <https://doi.org/10.1111/j.1365-246X.1984.tb01939.x>
- Coltice, N., Gérard, M., & Ulvrová, M. (2017). A mantle convection perspective on global tectonics. *Earth-Science Reviews*, *165*, 120–150. <https://doi.org/10.1016/j.earscirev.2016.11.006>
- Cramer, F., Shephard, G. E., & Heron, P. J. (2020). The misuse of colour in science communication. *Nature Communications*, *11*(1), 1–10. <https://doi.org/10.1038/s41467-020-19160-7>

- Dannberg, J., Eilon, Z., Faul, U., Gassmöller, R., Moulik, P., & Myhill, R. (2017). The importance of grain size to mantle dynamics and seismological observations. *Geochemistry, Geophysics, Geosystems*, 18(8), 3034–3061. <https://doi.org/10.1002/2017GC006944>
- Debayle, E., Kennett, B., & Priestley, K. (2005). Global azimuthal seismic anisotropy and the unique plate-motion deformation of Australia. *Nature*, 433(7025), 509–512. <https://doi.org/10.1038/nature03247>
- Debayle, E., & Ricard, Y. (2013). Seismic observations of large-scale deformation at the bottom of fast-moving plates. *Earth and Planetary Science Letters*, 376, 165–177. <https://doi.org/10.1016/j.epsl.2013.06.025>
- Garel, F., Thoraval, C., Tommasi, A., Demouchy, S., & Davies, D. R. (2020). Using thermo-mechanical models of subduction to constrain effective mantle viscosity. *Earth and Planetary Science Letters*, 539, 116243. <https://doi.org/10.1016/j.epsl.2020.116243>
- Hall, C. E., & Parmentier, E. (2003). Influence of grain size evolution on convective instability. *Geochemistry, Geophysics, Geosystems*, 4(3), 1029. <https://doi.org/10.1029/2002GC000308>
- Hedjazian, N., Garel, F., Davies, D. R., & Kaminski, E. (2017). Age-independent seismic anisotropy under oceanic plates explained by strain history in the asthenosphere. *Earth and Planetary Science Letters*, 460, 135–142. <https://doi.org/10.1016/j.epsl.2016.12.004>
- Hirth, G., & Kohlstedt, D. (2003). Rheology of the upper mantle and the mantle wedge: A view from the experimentalists. *Geophysical Monograph-American Geophysical Union*, 138, 83–106. <https://doi.org/10.1029/138GM06>
- Höink, T., Lenardic, A., & Richards, M. (2012). Depth-dependent viscosity and mantle stress amplification: Implications for the role of the asthenosphere in maintaining plate tectonics. *Geophysical Journal International*, 191(1), 30–41. <https://doi.org/10.1111/j.1365-246X.2012.05621.x>
- Holt, A. F., & Becker, T. W. (2016). The effect of a power-law mantle viscosity on trench retreat rate. *Geophysical Journal International*, 208(1), 491–507. <https://doi.org/10.1093/gji/ggw392>
- Jadamec, M., & Billen, M. (2010). Reconciling surface plate motions with rapid three-dimensional mantle flow around a slab edge. *Nature*, 465(7296), 338–341. <https://doi.org/10.1038/nature09053>
- Jadamec, M., & Billen, M. I. (2012). The role of rheology and slab shape on rapid mantle flow: Three-dimensional numerical models of the Alaska slab edge. *Journal of Geophysical Research*, 117(B2), B02304. <https://doi.org/10.1029/2011JB008563>
- Jain, C., Korenaga, J., & Karato, S.-I. (2018). On the grain size sensitivity of olivine rheology. *Journal of Geophysical Research: Solid Earth*, 123(1), 674–688. <https://doi.org/10.1002/2017JB014847>
- Jain, C., Korenaga, J., & Karato, S.-I. (2019). Global analysis of experimental data on the rheology of olivine aggregates. *Journal of Geophysical Research: Solid Earth*, 124(1), 310–334. <https://doi.org/10.1029/2018JB016558>
- Kang, K., Zhong, S., Geruo, A., & Mao, W. (2022). The effects of non-Newtonian rheology in the upper mantle on relative sea level change and geodetic observables induced by glacial isostatic adjustment process. *Geophysical Journal International*, 228(3), 1887–1906. <https://doi.org/10.1093/gji/ggab428>
- Karato, S.-I., & Wu, P. (1993). Rheology of the upper mantle: A synthesis. *Science*, 260(5109), 771–778. <https://doi.org/10.1126/science.260.5109.771>
- Kendall, E., Faccenda, M., Ferreira, A., & Chang, S.-J. (2022). On the relationship between oceanic plate speed, tectonic stress, and seismic anisotropy. *Geophysical Research Letters*, 49(15), e2022GL097795. <https://doi.org/10.1029/2022GL097795>
- King, S. D. (2016). An evolving view of transition zone and midmantle viscosity. *Geochemistry, Geophysics, Geosystems*, 17(3), 1234–1237. <https://doi.org/10.1002/2016GC006279>
- Korenaga, J., & Karato, S.-I. (2008). A new analysis of experimental data on olivine rheology. *Journal of Geophysical Research*, 113(B2), B02403. <https://doi.org/10.1029/2007JB005100>
- Li, M., & Zhong, S. (2019). Lateral motion of mantle plumes in 3-D geodynamic models. *Geophysical Research Letters*, 46(9), 4685–4693. <https://doi.org/10.1029/2018GL081404>
- Moresi, L.-N., & Solomatov, V. (1995). Numerical investigation of 2D convection with extremely large viscosity variations. *Physics of Fluids*, 7(9), 2154–2162. <https://doi.org/10.1063/1.868465>
- Neuharth, D., & Mittelstaedt, E. (2023). Temporal variations in plume flux: Characterizing pulsations from tilted plume conduits in a rheologically complex mantle. *Geophysical Journal International*, 233(1), 338–358. <https://doi.org/10.1093/gji/ggac455>
- Nicolas, A., & Christensen, N. I. (1987). Formation of anisotropy in upper mantle peridotites - A review. *Composition, Structure and Dynamics of the Lithosphere-Asthenosphere System*, 16, 111–123. <https://doi.org/10.1029/GD016p0111>
- Phipps Morgan, J., Morgan, W. J., Zhang, Y.-S., & Smith, W. H. (1995). Observational hints for a plume-fed, suboceanic asthenosphere and its role in mantle convection. *Journal of Geophysical Research*, 100(B7), 12753–12767. <https://doi.org/10.1029/95JB00041>
- Ranalli, G. (2001). Mantle rheology: Radial and lateral viscosity variations inferred from microphysical creep laws. *Journal of Geodynamics*, 32(4–5), 425–444. [https://doi.org/10.1016/S0264-3707\(01\)00042-4](https://doi.org/10.1016/S0264-3707(01)00042-4)
- Rolf, T., Capitanio, F. A., & Tackley, P. J. (2018). Constraints on mantle viscosity structure from continental drift histories in spherical mantle convection models. *Tectonophysics*, 746, 339–351. <https://doi.org/10.1016/j.tecto.2017.04.031>
- Rozel, A. (2012). Impact of grain size on the convection of terrestrial planets. *Geochemistry, Geophysics, Geosystems*, 13(10), Q10020. <https://doi.org/10.1029/2012GC004282>
- Schulz, F., Tosi, N., Plesa, A.-C., & Breuer, D. (2020). Stagnant-lid convection with diffusion and dislocation creep rheology: Influence of a non-evolving grain size. *Geophysical Journal International*, 220(1), 18–36. <https://doi.org/10.1093/gji/ggz417>
- Semple, A., & Lenardic, A. (2020). The robustness of pressure-driven asthenospheric flow in mantle convection models with plate-like behavior. *Geophysical Research Letters*, 47(17), e2020GL089556. <https://doi.org/10.1029/2020GL089556>
- Semple, A., & Lenardic, A. (2021). Feedbacks between a non-Newtonian upper mantle, mantle viscosity structure and mantle dynamics. *Geophysical Journal International*, 224(2), 961–972. <https://doi.org/10.1093/gji/ggaa495>
- Solomatov, V. (1995). Scaling of temperature-and stress-dependent viscosity convection. *Physics of Fluids*, 7(2), 266–274. <https://doi.org/10.1063/1.868624>
- Stein, C., Schmalz, J., & Hansen, U. (2004). The effect of rheological parameters on plate behaviour in a self-consistent model of mantle convection. *Physics of the Earth and Planetary Interiors*, 142(3–4), 225–255. <https://doi.org/10.1016/j.pepi.2004.01.006>
- Tackley, P. J. (2000a). Self-consistent generation of tectonic plates in time-dependent, three-dimensional mantle convection simulations. *Geochemistry, Geophysics, Geosystems*, 1(8), 1021. <https://doi.org/10.1029/2000GC000036>
- Tackley, P. J. (2000b). Self-consistent generation of tectonic plates in time-dependent, three-dimensional mantle convection simulations 2. Strain weakening and asthenosphere. *Geochemistry, Geophysics, Geosystems*, 1(8). <https://doi.org/10.1029/2000GC000043>
- Tackley, P. J. (2008). Modelling compressible mantle convection with large viscosity contrasts in a three-dimensional spherical shell using the yin-yang grid. *Physics of the Earth and Planetary Interiors*, 171(1–4), 7–18. <https://doi.org/10.1016/j.pepi.2008.08.005>
- Tosi, N., & Padovan, S. (2021). Mercury, moon, Mars. In *Mantle convection and surface expressions* (pp. 455–489). American Geophysical Union (AGU). <https://doi.org/10.1002/9781119528609.ch17>

- Trompert, R., & Hansen, U. (1998). Mantle convection simulations with rheologies that generate plate-like behaviour. *Nature*, 395(6703), 686–689. <https://doi.org/10.1038/27185>
- Weller, M. B., & Lenardic, A. (2018). On the evolution of terrestrial planets: Bi-Stability, stochastic effects, and the non-uniqueness of tectonic states. *Geoscience Frontiers*, 9(1), 91–102. <https://doi.org/10.1016/j.gsf.2017.03.001>